

Critical-Element-Free Permanent-Magnet Materials Based on Ce₂Fe₁₄B

Li Yin^{1,2,*}, Jiaqiang Yan^{1,2}, Brian C. Sales^{1,2}, and David S. Parker^{1,2}

¹Material Science and Technology Division, Oak Ridge National Laboratory, Oak Ridge, Tennessee 37831, USA

²Critical Materials Institute, Ames, Iowa 50011, USA



(Received 9 February 2022; revised 2 May 2022; accepted 18 May 2022; published 9 June 2022)

Developing a critical-element-free low-cost permanent magnet is an urgent necessity in view of rapidly developing technologies and the associated huge market demand for Nd₂Fe₁₄B-based magnets. Here, inspired by the abundant and low-cost nature of Ce and these high-performance Nd₂Fe₁₄B permanent magnets, we explore whether it is in fact possible to attain a useful performance in alloys based on the sister material Ce₂Fe₁₄B, employing both experimental and theoretical efforts. Experimentally, we study Ce₂Fe₁₄B with Co, La, and Zr substitutions. The Zr substitution is explored in view of Zr's frequent role in enhancing magnetic anisotropy in permanent magnets, while the Co and La substitutions serve to remedy the too-low Curie point of 433 K in the base alloy. While we find no Zr-related anisotropy enhancement either experimentally or theoretically, the cosubstitution of La and Co indeed improves the Curie temperature as well as the magnetization, M_s , with a potential energy product as high as 38 MG Oe. These properties together suggest optimization of the alloy LaCeFe_{12.7}Co_{1.3}B (with only 7 wt % cobalt) as a critical-element-free permanent magnet. While the substituted elements do not enhance magnetic anisotropy, from theory, we find a substantial increase, to a first anisotropy constant, K_1 , as high as 4.24 MJ/m³, associated with Bi substitution for Ce. Our experimental and theoretical results demonstrate the great potential of La, Co, and Bi substitutions in developing low-cost and critical-element-free Ce₂Fe₁₄B-based permanent magnets.

DOI: 10.1103/PhysRevApplied.17.064020

I. INTRODUCTION

Permanent magnets have been widely studied for the last three decades [1–3], owing to their widespread applications and rapidly increasing global market demand. To date, permanent magnets can be roughly distinguished to fall into three groups: the Nd₂Fe₁₄B and Sm-Co-based high-performance rare-earth magnets, the relatively low performance ferrite magnet, and the alnico-represented intermediate-gap magnet [4,5]. Especially, the extremely critical and expensive Dy is essential to fix the anisotropy deterioration at high temperature in industrial Nd₂Fe₁₄B. Considering the availability and commercial demand for critical elements such as Nd and Dy, it is of urgent importance to find abundant and low-cost magnets. In general, rare-earth elements are generally considered to be essential for high-performance permanent magnets, with Nd and Sm providing most of the crucial magnetic anisotropy in the aforementioned rare-earth magnet. Recent work by the U.S. Department of Energy funded Critical Materials Institute, however, has demonstrated [6–9] that cerium can also serve this purpose. In particular, more and more Ce-based magnets have been proposed in recent years, such as the

CeCo₅ [6], CeCo₃ [7], and Ce₂Co₁₇ systems [9]. These findings inspire us to search for other Ce-based permanent magnets with high performance. Moreover, instead of employing the relatively expensive Co element, we choose the low-cost Fe element to search for the potential high performance of Ce-Fe compounds. Fe atoms generally carry a larger local moment than Co atoms, making this an advantageous choice from a performance perspective as well.

Among Ce-based magnets [10], Ce₂Fe₁₇ and Ce₂Fe₁₄B are distinct owing to their strong magnetization over 1.4 T at low temperature [3,11]. As in several other Ce-based magnets, Ce₂Fe₁₇ and Ce₂Fe₁₄B also have the drawback of undesirably planar, or smaller-than-optimal, magnetocrystalline anisotropy. In Ce₂Fe₁₇, the magnetocrystalline anisotropy is planar with a value of about -2.2 MJ/m³ [12–14]. Although iridium substitution of Ce₂Fe₁₇ is demonstrated to induce a substantial uniaxial anisotropy [11], the cost increase associated with iridium is adverse to our pursuit for a low-cost permanent magnet. However, intrinsic Ce₂Fe₁₄B shows uniaxial magnetocrystalline anisotropy, which is one of the crucial properties for a permanent magnet. Given the smaller-than-optimal magnetocrystalline anisotropy of 1.52 MJ/m³ [3], we devote our efforts towards improving this value for Ce₂Fe₁₄B, for better performance as a permanent magnet.

* yinl@ornl.gov

Atomic substitution is a time-honored effective method to modulate the magnetic properties, especially for permanent magnets [1,3]. To date, different kinds of atom substitutions on Ce and Fe sites have been studied for $\text{Ce}_2\text{Fe}_{14}\text{B}$. These substitutions can improve the saturation magnetization and Curie point of $\text{Ce}_2\text{Fe}_{14}\text{B}$, such as La substitution of Ce [15] and Co, Ni, or Si substitution of Fe [16]. Ni, Si, or Al substitution decreases both the magnetization and magnetic anisotropy [16]. Moreover, La substitution can also suppress the formation of the undesired magnetically soft CeFe_2 Laves phase [15]. The microstructure of $\text{Ce}_2\text{Fe}_{14}\text{B}$ can also be optimized by Zr and Hf doping [17]. However, in terms of magnetocrystalline anisotropy, only the Zr substitution of Ce has ever been reported to enhance the anisotropy of $\text{Ce}_2\text{Fe}_{14}\text{B}$ and other $\text{R}_2\text{Fe}_{14}\text{B}$ compounds [18,19]. These limiting results motivate us to explore the origin of anisotropy in $\text{Ce}_2\text{Fe}_{14}\text{B}$.

Here, we experimentally study $\text{Ce}_2\text{Fe}_{14}\text{B}$ with Co, La, or Zr substitutions. Along with the Co substitutions of Fe, partial Zr substitution increases the impurity phase and has little effect on the Curie point and M_s . While, without loss of the anisotropy field, the La substitution of Ce increases the Curie temperature and saturation magnetization, which may produce an estimated energy product of 38 MG Oe. These properties enable $\text{LaCeFe}_{12.7}\text{Co}_{1.3}\text{B}$ as a potential critical-element-free high-performance permanent magnet. While neither La nor Zr substitution improves the magnetic anisotropy of $\text{Ce}_2\text{Fe}_{14}\text{B}$, we further use first-principles calculations to study the origin of magnetic anisotropy in $\text{Ce}_2\text{Fe}_{14}\text{B}$. It is found that, contrary to the prevailing view of cerium in $\text{Ce}_2\text{Fe}_{14}\text{B}$ as nonmagnetic and therefore not contributing to magnetic anisotropy [3], the magnetic anisotropy in $\text{Ce}_2\text{Fe}_{14}\text{B}$ is comparably contributed to by the Ce and Fe atoms, where the Ce-projected magnetic anisotropy is predominately provided by the Ce atoms at the 4g site. This is analogous to previous studies [20], which demonstrated similar behavior of Nd in $\text{Nd}_2\text{Fe}_{14}\text{B}$ and reminded us of the importance of magnetically nonequivalent sites for anisotropy engineering. We further employ the atom substitution on the “noncontributing” 4f-site Ce atoms (the energetically favorable site for Bi) and find a considerable, almost 3 times, promotion of magnetic anisotropy in Bi-substituted $\text{Ce}_2\text{Fe}_{14}\text{B}$, while slightly increasing the already strong magnetization. These experimental and calculation results reveal the great potential of La-Co cosubstitution and Bi substitution on developing a $\text{Ce}_2\text{Fe}_{14}\text{B}$ -based low-cost and critical-element-free permanent magnet.

II. EXPERIMENTAL AND CALCULATION METHODS

The $\text{Ce}_2\text{Fe}_{14}\text{B}$ -based materials are prepared via the conventional arc melting and postannealing process. The

starting materials are La (Ames Laboratory), Ce (Ames Laboratory), Zr (Alfa Aesar, 99.8%), Fe pieces (Alfa Aesar, 99.999%), Co ingots (Alfa Aesar, 99.999%), and B pieces (Alfa Aesar, 99.5%). The starting materials in the desired ratio are arc melted in an argon-arc furnace with a water-cooled hearth and a nonconsumable tungsten electrode. The ingot is melted 4 or 5 times to ensure inhomogeneity and then sealed in a quartz tube under vacuum. The ampoule is then kept in a box furnace at 920 °C for 15 days. The above annealing temperature and time are found to give samples with the highest fraction of 2-14-1 phase. After the long-term annealing, the ampoule is quenched in iced water. Room-temperature x-ray powder-diffraction measurements are performed using a PANalytical X’Pert diffractometer and a position-sensitive detector using monochromated Cu $K\alpha 1$ radiation.

The field dependence of magnetization is measured at room temperature for both aligned powder and a small piece of annealed polycrystalline ingot. Fine powder is aligned with epoxy inside of a capsule using a procedure described previously [21]. The magnetic ordering temperature is determined using a Perkin-Elmer 7 series thermogravimetric analyzer with a permanent magnet positioned right above the sample. A dramatic apparent mass change is expected at the Curie temperature because the force exerted on the sample by the magnet disappears above the Curie temperature.

The calculations are performed by using the all-electron-density functional code WIEN2k [22,23] with the generalized-gradient approximation of Perdew, Burke, and Ernzerhof [24]. The linearized augmented plane wave (LAPW) method is employed [25]. The RK_{\max} produced by the smallest LAPW sphere radius (R) and the interstitial plane-wave cutoff (K_{\max}) is set as 7.0 for good convergence. $\text{Ce}_2\text{Fe}_{14}\text{B}$ is in the space group of $P4_2/mnm$ (136) [3,26], with two inequivalent kinds of Ce. Here, the lattice constants of $\text{Ce}_2\text{Fe}_{14}\text{B}$ are fixed to its experimental values of $a = b = 8.778 \text{ \AA}$ and $c = 12.094 \text{ \AA}$ [27]. The internal atomic coordinates are relaxed until forces on all the atoms are less than 1 mRy/bohr, with the 200 \mathbf{k} points in the full Brillouin zone. The magnetic anisotropy energy (MAE) is calculated with spin-orbit coupling (SOC) and assumed collinear spin arrangement. MAE is defined as $(E_{[110]} - E_{[001]})/V$, where $E_{[110]}$ and $E_{[001]}$ are the total energies of the system for magnetization oriented along the [110] and [001] directions, respectively. V denotes the volume of the primitive cell. The positive (negative) value of the MAE indicates the out-of-plane (in-plane) magnetic anisotropy. In MAE calculations, the charge-convergence criterion is 0.0001 e , and 400 \mathbf{k} points are applied in the full Brillouin zone. Considering that the MAE is highly sensitive to the employed \mathbf{k} points, we calculate the MAE of $\text{Ce}_2\text{Fe}_{14}\text{B}$ with 400 and 600 \mathbf{k} points, which produces a small difference of 1.70%. The $E_{[110]}$ ($E_{[001]}$) calculated with 400 and 600 \mathbf{k} points shows an energy difference

of 0.726 meV/f.u. (0.763 meV/f.u.). So, 400 \mathbf{k} points are applied in the pristine and substituted $\text{Ce}_2\text{Fe}_{14}\text{B}$. To check the ability to resist self-demagnetization, the magnetic hardness parameters of substituted $\text{Ce}_2\text{Fe}_{14}\text{B}$ are calculated as $\kappa = \sqrt{K_1}/(\mu_0 M_s^2)$ [4,8,29], where K_1 indicates the magnetocrystalline anisotropy energy (i.e., the calculated MAE in this work), M_s denotes the saturation magnetization, and μ_0 is the vacuum permeability of $4\pi \times 10^{-7}$ T m/A. The crystal structure and charge density are visualized in VESTA 3.4.7 [30].

The formation enthalpies and decomposition enthalpies of substituted $\text{Ce}_2\text{Fe}_{14}\text{B}$ are calculated in the Vienna *ab initio* simulation package [31,32]. The projector-augment-wave pseudopotentials and generalized-gradient approximation are employed in the calculations [33,34]. The pseudopotential of elementary substances and binary and ternary materials with Ce, Bi, Fe, or B atoms are the same as the pseudopotential of substituted $\text{Ce}_2\text{Fe}_{14}\text{B}$. The plane-wave energy cutoff is 520 eV. The convergence criteria for the energy and atomic forces are set to 10^{-6} eV and 0.001 eV/Å, respectively.

III. RESULTS AND DISCUSSION

A. Experimental analysis of $\text{Ce}_2\text{Fe}_{14}\text{B}$ with Co, La, and Zr substitution

In general, the Curie point of $\text{R}_2\text{Fe}_{14}\text{B}$ can be improved by Co substitution for Fe [3,35,36]. According to previous results [37], the Curie temperature in $\text{Ce}_2\text{Fe}_{14}\text{B}$ increases with the Co content, reaching 586 K with a Co content of about 15%. So, we start with Co substitution here. The anisotropy field of $\text{Ce}_2\text{Fe}_{14}\text{B}$ is around 3 T and the saturation magnetization is 130 emu/g at room temperature. Partial substitution of Fe by Co in $\text{Ce}_2\text{Fe}_{14-x}\text{Co}_x\text{B}$ increases the saturation moment with x up to 2.5 but reduces the anisotropy field when $x > 1.5$ [37]. We thus study the effect of partial substitution of Ce by La and Zr in $\text{Ce}_2\text{Fe}_{14-x}\text{Co}_x\text{B}$ with $x = 1.3$ or 2.0.

According to the x-ray powder diffraction of $\text{Ce}_{2-x}\text{Zr}_x\text{Fe}_{12}\text{Co}_2\text{B}$ collected at room temperature, for $x = 0$, $\text{Ce}_2\text{Fe}_{12}\text{Co}_2\text{B}$ is the majority phase with a small fraction of $\text{Ce}_2\text{Fe}_{17}$ that can barely be resolved by diffraction measurements. The lattice parameters determined from Rietveld refinement are $a = 8.7509(10)$ Å and $c = 12.0824(16)$ Å, consistent with previous reports [38]. Partial substitution of Ce by Zr significantly increases the fraction of $\text{Ce}_2\text{Fe}_{17}$. The fraction of $\text{Ce}_2\text{Fe}_{17}$ increases from 13 wt% for $\text{Ce}_{1.9}\text{Zr}_{0.1}\text{Fe}_{12}\text{Co}_2\text{B}$ to 64 wt% for $\text{Ce}_{1.8}\text{Zr}_{0.2}\text{Fe}_{12}\text{Co}_2\text{B}$. The lattice parameters for the 2-14-1 phase are $a = 8.7481(4)$ Å and $c = 12.0692(6)$ Å for both $x = 0.1$ and 0.2.

Replacing half of Ce by La seems to stabilize the desired 2-14-1 phase. As shown in Fig. 1, 2-14-1 is the majority phase in all $(\text{LaCe})_{2-x}\text{Zr}_x\text{Fe}_{12.7}\text{Co}_{1.3}\text{B}$ samples. From room-temperature x-ray powder diffraction, the impurity

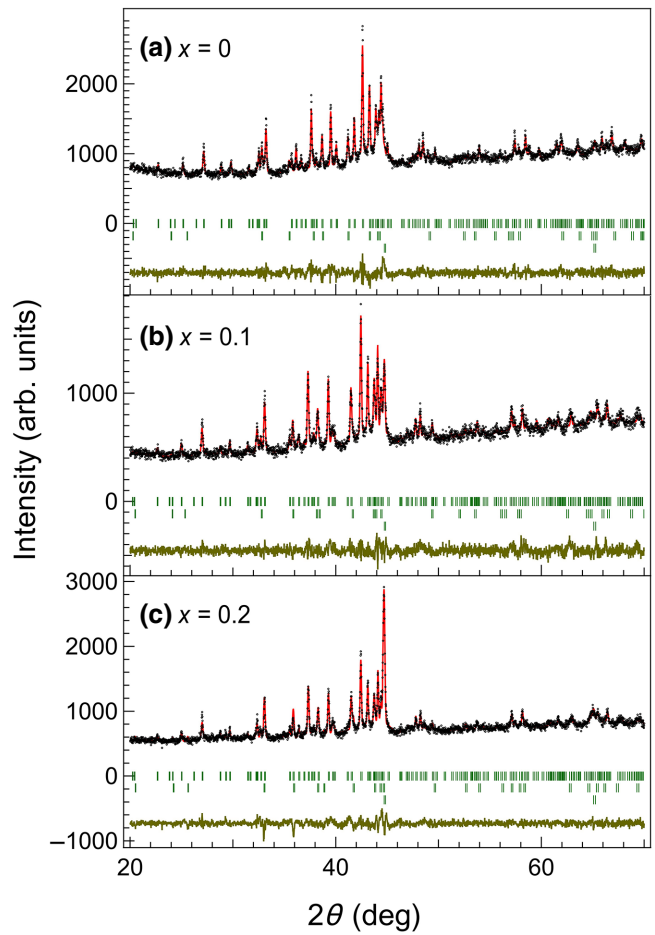


FIG. 1. Rietveld fit of the room-temperature X-ray powder-diffraction patterns of $(\text{LaCe})_{2-x}\text{Zr}_x\text{Fe}_{12.7}\text{Co}_{1.3}\text{B}$: (a) $x = 0.0$, (b) $x = 0.1$, and (c) $x = 0.2$. Observed (open symbols), calculated (line), and difference (bottom solid line) profiles are shown. Vertical ticks correspond to the position of calculated Bragg peaks of all phases [from top to bottom, 2-14-1, CeFe_3CoB , and $\text{Fe}(\text{Co})$].

phases are identified as $\text{Fe}(\text{Co})$ and CeFe_3CoB . While the fraction of CeFe_3CoB can be comparable in different compositions, the amount of $\text{Fe}(\text{Co})$ impurity increases significantly with increasing amount of Zr. There are 13 wt% of $\text{Fe}(\text{Co})$ impurities in $x = 0.1$ and 24 wt% in $x = 0.2$, both are higher than 1.7 wt% in samples without any Zr in the starting materials. Partial substitution of Ce by La expands the c lattice of the 2-14-1 phase. The lattice parameters are $a = 8.7472(6)$ Å, $c = 12.2244(10)$ Å for $x = 0.1$, to $a = 8.7773(6)$ Å, $c = 12.193(1)$ Å for $x = 0.2$, as determined from the Rietveld refinement of the room-temperature powder-diffraction patterns. Overall, partial substitution of Zr increases the amount of impurity phase, and La substitution stabilizes the desired 2-14-1 phase.

We determine the magnetic ordering temperature, i.e., the Curie temperature, by magnetic thermogravimetric analyses. The Curie temperature for $\text{Ce}_{2-x}\text{Zr}_x\text{Fe}_{12}\text{Co}_2\text{B}$ is at 558 K and the partial substitution of Ce by Zr has

little effect on the Curie temperature. With half of Ce replaced by La, the Curie point is increased to 588 K for $(\text{La}_{0.5}\text{Ce}_{0.5})_{1.9}\text{Zr}_{0.1}\text{Fe}_{12}\text{Co}_2\text{B}$, which is higher than the Curie point of about 490 K (~ 523 K) achieved in $\text{Ce}_2\text{Fe}_{14}\text{B}$ substituted just by La (Co) [15,37]. This 588-K value is, in fact, equivalent to that of $\text{Nd}_2\text{Fe}_{14}\text{B}$. Figure 2(a) shows the field dependence of magnetization to determine M_s at room temperature. M_s for $\text{Ce}_2\text{Fe}_{12}\text{Co}_2\text{B}$ is about 120 emu/g, which is comparable to that of $\text{Ce}_2\text{Fe}_{14}\text{B}$ reported previously [37]. Partial substitution of Ce by Zr in $\text{Ce}_{2-x}\text{Zr}_x\text{Fe}_{12}\text{Co}_2\text{B}$ has little effect on M_s . In contrast, replacing half of Ce by La increases M_s to 145 emu/g (or 1.38 T) in $\text{LaCeFe}_{12.7}\text{Co}_{1.3}\text{B}$. It should be noted that further introducing Zr into the La-Ce compound also has little effect on M_s [please see $(\text{LaCe})_{2-x}\text{Zr}_x\text{Fe}_{12.7}\text{Co}_{1.3}\text{B}$ ($x = 0.1$ or 0.2) in Fig. 2(a)]. Meanwhile, the M_s of 1.38 T in $\text{LaCeFe}_{12.7}\text{Co}_{1.3}\text{B}$ at room temperature is higher than the M_s of about 1.15 T in $\text{LaCeFe}_{14}\text{B}$ at 300 K [15], implying the importance of La and Co cosubstitutions.

We also analyze the anisotropy field for these La- and Zr-substituted compounds. Figure 2(b) shows the field dependence of magnetization of aligned powder in order to determine the anisotropy field. It can be found that the anisotropy field remains the same when half of Ce is replaced by La. With partial substitution of Ce by Zr, H_A is gradually suppressed. Given these experimental results, partial Zr substitution increases the impurity phase and has little effect on the Curie point and M_s . While, the substitution of La improves the Curie temperature and M_s without loss of the anisotropy field, which may produce an energy product as high as 38 MG Oe, as estimated by 80% of $(M_s)^2/4$. For comparison, the highest-performing $\text{Nd}_2\text{Fe}_{14}\text{B}$ grades, at 55 MG Oe, achieve approximately 86% of the theoretical maximum of 64 MG Oe, based upon an M_s value of 1.6 T. These properties enable $\text{LaCeFe}_{12.7}\text{Co}_{1.3}\text{B}$ to be a potential permanent magnet without critical elements and just 7 wt % of cobalt.

B. Computational study on the origin of magnetic anisotropy in $\text{Ce}_2\text{Fe}_{14}\text{B}$

Although we achieve permanent-magnet properties in $\text{Ce}_2\text{Fe}_{14}\text{B}$ with La and Co cosubstitution, it should be noted that neither La nor Zr substitution improves the magnetic anisotropy of $\text{Ce}_2\text{Fe}_{14}\text{B}$. As we mention in Sec. I, only the Zr substitution of Ce is reported to enhance the anisotropy of $\text{Ce}_2\text{Fe}_{14}\text{B}$ and other $\text{R}_2\text{Fe}_{14}\text{B}$ compounds [18,19], which is contrary to our experimental results. These experimental results reflect the challenge of modulating the magnetic anisotropy of $\text{Ce}_2\text{Fe}_{14}\text{B}$. Here, we employ theoretical calculations to continue the exploration of $\text{Ce}_2\text{Fe}_{14}\text{B}$.

To perform a “reality check” on our magnetic calculations in $\text{Ce}_2\text{Fe}_{14}\text{B}$, we first calculate its magnetization and magnetic anisotropy and compare the calculated values

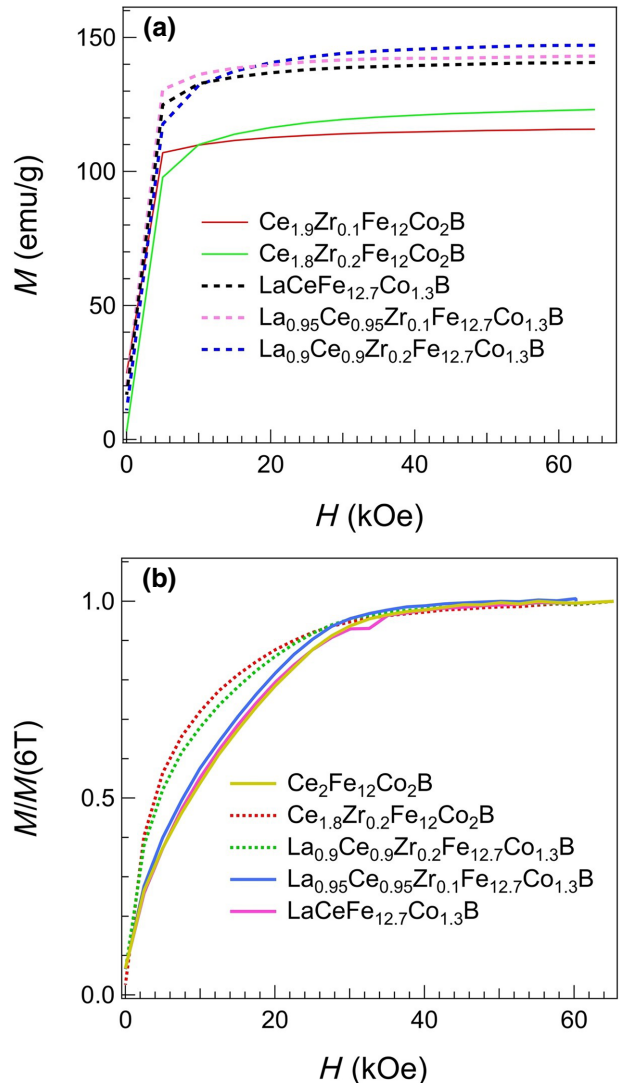


FIG. 2. (a) Field dependence of magnetization for $\text{Ce}_2\text{Fe}_{14}\text{B}$ with La and Zr substitutions, to determine the saturation magnetization at room temperature. (b) Field dependence of magnetization of aligned powder with magnetic field applied along the hard direction. Measurements are performed at room temperature.

with experimental results. The calculated magnetization is 1.53 T and the magnetic anisotropy is found to be 1.42 MJ/m^3 . On this basis, we obtain an anisotropy field, H_A , of 2.34 T from the relationship of $\mu_0 H_A = 2\mu_0 K_1/M_s$. In previously reported experiments [3], the magnetization of 1.47 T and anisotropy field of 2.6 T are measured at 4 K in $\text{Ce}_2\text{Fe}_{14}\text{B}$. It can be seen that the calculated magnetization of 1.53 T and anisotropy field of 2.34 T are relatively close to the related experimental values. So, our calculation should be reliable, and we continue to explore the origin of magnetic anisotropy in $\text{Ce}_2\text{Fe}_{14}\text{B}$.

As shown in Fig. 3(a), $\text{Ce}_2\text{Fe}_{14}\text{B}$ holds two inequivalent kinds of Ce, which lie in the $4f$ and $4g$ sites. Here, we name the two kinds of Ce as Ce $4f$ and Ce $4g$. The

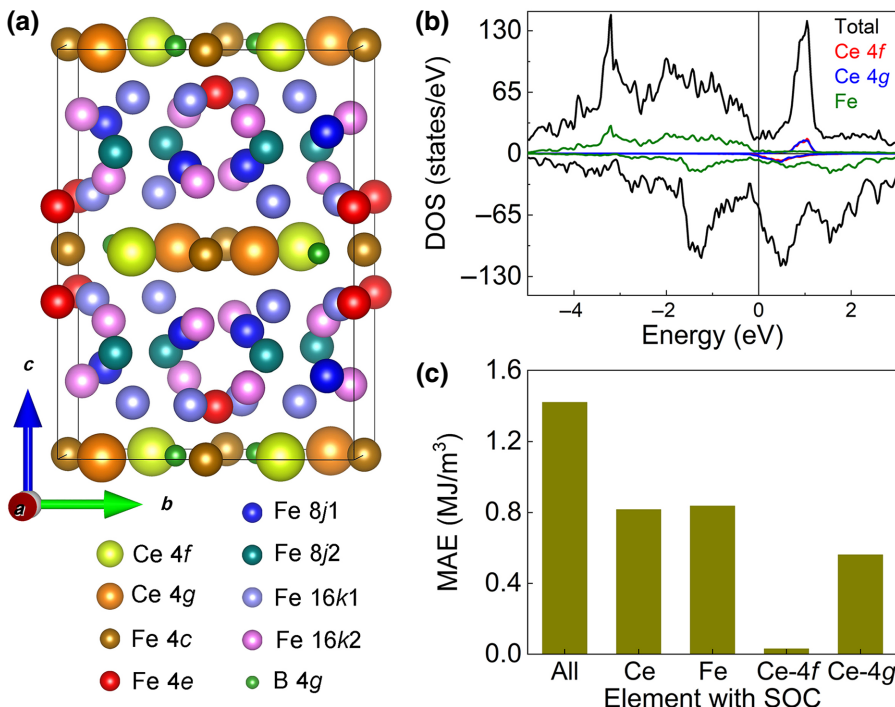


FIG. 3. (a) Side-view geometry structures of Ce₂Fe₁₄B. Two kinds of Ce and six kinds of Fe and B atoms in Ce₂Fe₁₄B are marked with different colored balls. (b) Total DOS, *f*-orbital DOS of inequivalent Ce atoms, and *d*-orbital DOS of Fe atoms in Ce₂Fe₁₄B. Ce 4*f* (Ce 4*g*) label denotes Ce atoms in the 4*f* (4*g*) site, as marked in (a). *d*-Orbital DOS of Fe atom is averaged over *d*-orbital DOS of all sites of Fe atoms. Positive and negative values on the vertical axis denote spin-up and spin-down channels, respectively. Fermi level is 0 eV. (c) MAE calculated with SOC employed in different atoms of Ce₂Fe₁₄B.

total and projected density of states (DOS) in Ce₂Fe₁₄B are shown in Fig. 3(b). It is found that the majority of *f*-orbital states are located above the Fermi level, which is associated with the smaller number of 4*f* electrons in Ce, as compared with other rare-earth elements. To analyze the origin of magnetic anisotropy in Ce₂Fe₁₄B, we employ the second-variational method to switch on the SOC for specific atoms, calculating the corresponding atom-projected MAE. As displayed in Fig. 3(c), the MAE in Ce₂Fe₁₄B is comparably contributed to by the Ce and Fe atoms. Then, the MAE of Ce is predominantly contributed to by Ce atoms at the 4*g* site, which is 18 times larger than the MAE contributed to by Ce 4*f*. Such a phenomenon is similar to that observed in Nd₂Fe₁₄B [20]. However, as shown in Fig. 3(b), the *f*-orbital DOS of inequivalent Ce 4*f* and Ce 4*g* are highly similar to each other. Given the inequivalent sites and dramatically different MAE contribution of Ce-4*f* and Ce-4*g* atoms, we further calculate the partial DOS projected on the two kinds of Ce atoms, as shown in Figs. 4(a) and 4(b). It should be noted that the sum of Ce- and Fe-contributed MAE is 1.65 MJ/m³, which is slightly larger than, although comparable to, the MAE of 1.42 MJ/m³ calculated with SOC in all of the atoms. The added Ce-4*f*- and Ce-4*g*-contributed MAE of 0.59 MJ/m³ is also different from the Ce-contributed MAE of 0.82 MJ/m³. Such a phenomenon is due to the inaccurate orbital distribution. Generally, all the electrons in the whole material will be employed with SOC, including those interstitial electrons between two atoms. However, as part of the atoms are employed with SOC, those interstitial electrons will cause differences due

to the inaccurate orbital distribution between atoms with and without SOC, which will be inevitable in the partial SOC calculations. Here, the differences between the summed MAE and directly calculated MAE are 14% and 28% in the two cases. So, although the atom-projected MAE indicates the presence of cross terms in the magnetic anisotropy, it is still helpful to analyze the origin of magnetic anisotropy in Ce₂Fe₁₄B.

In Figs. 4(a) and 4(b), the *f*-projected DOS is totally different in Ce-4*f* and Ce-4*g* atoms, especially around the Fermi level. In the Ce-4*f* atom, maximum occupation near the Fermi level comes from the *f*_{z3} states, as shown by the bold green line in Fig. 4(a). However, in the Ce-4*g* atom, the *f*_{xz2} states contribute predominately to the occupied *f* states [see the bold magenta line in Fig. 4(b)]. Meanwhile, as shown in the gray section in Figs. 4(a) and 4(b), the *f*_{xz2}-projected DOS in the Ce-4*g* atom is also larger than the *f*_{z3}-projected DOS in the Ce-4*f* atom, underlining that the Ce-4*g* atom contains more *f* electrons than the Ce-4*f* atom. These results are consistent with the mixed valence of Ce demonstrated in experiments [39–41]. More *f* electrons provide a foundation for achieving a large magnetic anisotropy in the Ce-4*g* atom. Additionally, we note that the *f*_{xz2} state in the Ce-4*g* atom is mainly occupied in the energy interval of [E_F–0.2 eV, E_F], where E_F denotes the Fermi level. However, in that energy window, the *p*-orbital DOS of the B atom mainly comes from the *p*_x orbital, which is capable of hybridizing with the *f*_{xz2} state in the Ce-4*g* atom. Herewith, the DOS in Figs. 3(b), 4(a), and 4(b) show the number of states in a specific energy level. To check the B-Ce interaction, we further plot the electron

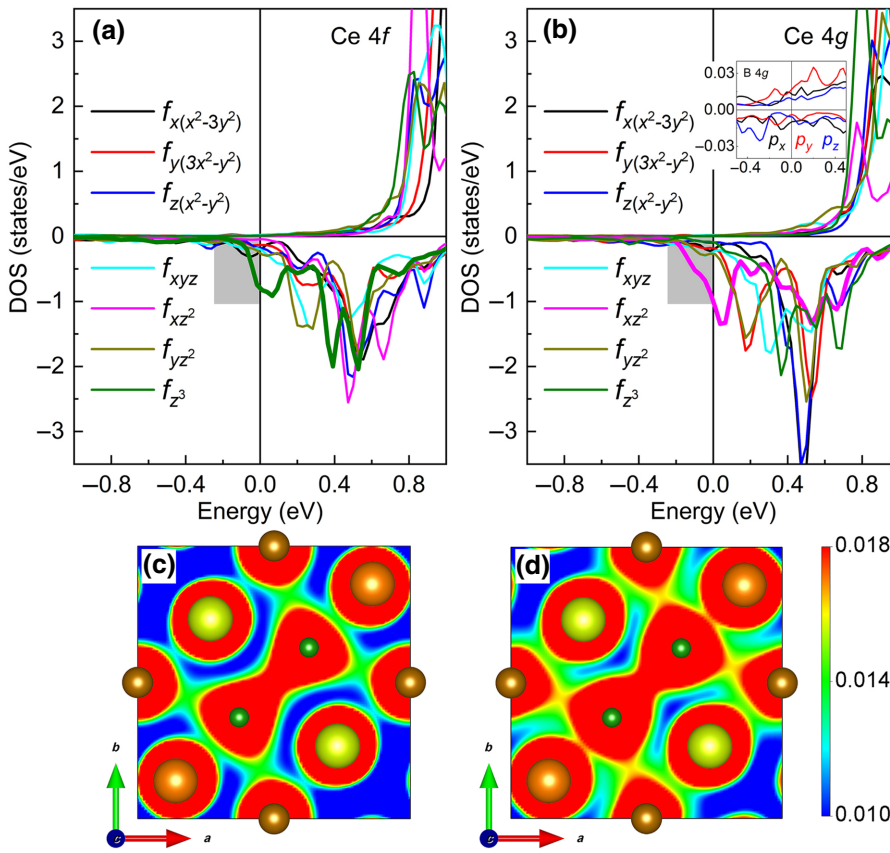


FIG. 4. Partial DOS projected on f states of (a) Ce-4*f* and (B) Ce-4*g* atoms in Ce₂Fe₁₄B. Fermi level is 0 eV. Inset of (b) denotes the spin-polarized partial DOS projected on the p states of B atoms. (c),(d) Spin-up and spin-down electron densities projected along the (001) plane at a spatial distance of 1.0*c*, where *c* is the *z*-directional lattice constant of Ce₂Fe₁₄B. Value of electron density in (c),(d) is depicted as the color bar.

density for Ce₂Fe₁₄B, displaying the electrons in a specific position. As shown in Figs. 4(c) and 4(d), the electron densities between B and Ce-4*g* atoms are larger than that between B and Ce-4*f* atoms. B atoms prefer to interact with Ce-4*g* atoms by orbital hybridization, which is consistent with the discussed DOS results. Notably, the distance between B and its nearest Ce-4*f* atom is 3.26 Å, which is larger than the distance of 2.89 Å between B and its nearest Ce-4*g* atom. The preferred interaction between B and Ce 4*g* is favored by such a structural feature.

C. Magnetic anisotropy improved by 4*f*-site atom substitution

According to the atom-projected MAE in Fig. 3(c), only a small portion of Ce-projected magnetic anisotropy in Ce₂Fe₁₄B originates from the Ce-4*f* site. So, with the aim of improving the magnetic anisotropy in Ce₂Fe₁₄B, we try atom substitution of the Ce-4*f* site. In this work, Sn, Sb, Bi, Ca, and Sr are considered. To determine the preference site of introduced atoms, we calculate the total energies, E_{4f} (E_{4g}), of (Ce_{0.75}*X*_{0.25})₂Fe₁₄B (*X* = Sn, Sb, Bi, Ca, or Sr), as the *X* atom occupies the 4*f* (4*g*) site of rare-earth atom. The relative energy of E_{4f} with respect to E_{4g} reflects the preference sites of the *X* atom, where a negative (positive) value of relative energy indicates the preferred 4*f* (4*g*) site. The symmetry of Ce₂Fe₁₄B is not damaged by

atom substitution. As displayed in Fig. 5(a), differently from Ca, Sr, or La, Sn, Sb, Pb, and Bi prefer to occupy the 4*f* site. Such a phenomenon should be associated with the atomic volumes. For reference, the atomic volumes of Ce, Sn, Sb, Pb, Bi, Ca, Sr, La, and Zr are 20.69, 16.29, 18.19, 18.26, 21.31, 26.20, 33.94, 22.39, and 14.02 cm³/mol at atmospheric pressure and room temperature [42]. So, it is noted that Sn, Sb, Pb, Bi, and Zr atoms with smaller than or comparable atomic volumes to that of Ce prefer to occupy the 4*f* site. Then, Ca, Sr, and La atoms with larger atomic volumes than Ce show the preference of the 4*g* site. The atomic-volume-related preference site is attributed to the structure of Ce₂Fe₁₄B. In the 2:14:1 structure, the Ce-4*f* and Ce-4*g* atoms are located at different Fe environments with six inequivalent Fe sites [Fig. 3(a)]. For the Ce-4*f* atom, its distances to the nearest Fe atoms in 4*c*, 4*e*, and 16*k*₂ sites are 3.11, 3.20, and 3.04 Å, respectively, which are smaller than the corresponding distances (3.37, 4.63, and 3.26 Å) of the Ce-4*g* atom to its nearest Fe atoms at the 4*c*, 4*e*, and 16*k*₂ sites. As compared with the 4*f* site, the 4*g* site provides a bigger space with a large distance to Fe atoms. Hence, in substituted Ce₂Fe₁₄B, the atom with a larger volume than that of Ce prefers to occupy the 4*g* site.

Next, we explore the magnetic properties of (Ce_{0.75}*X*_{0.25})₂Fe₁₄B (*X* = Sn, Sb, Pb, Bi, La, or Zr), where *X* atoms, except the La atom, occupy the 4*f* site. As shown in Fig. 5(b), the magnetic anisotropy of Ce₂Fe₁₄B is

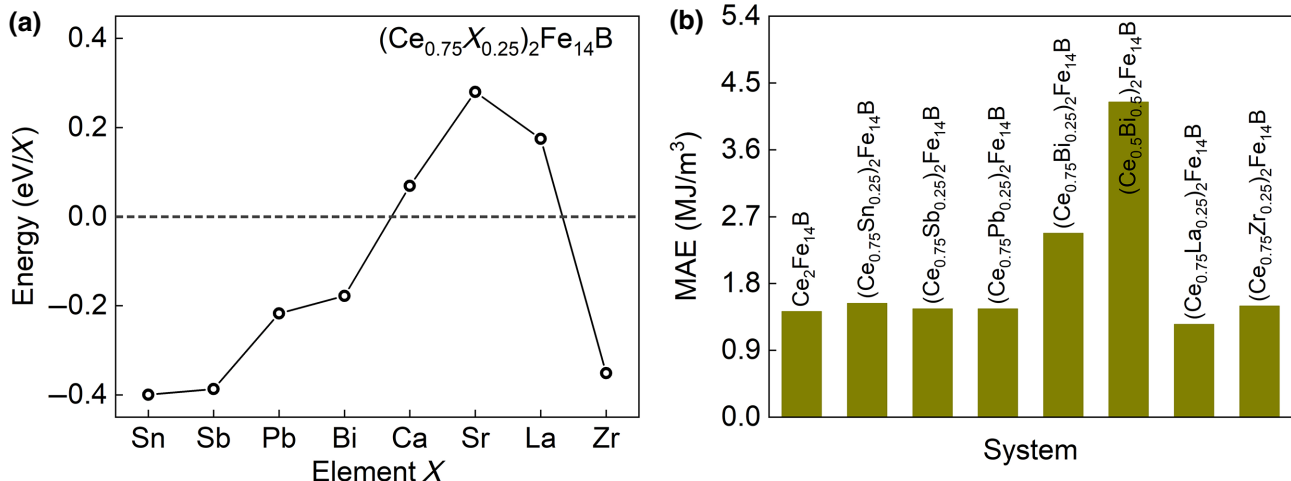


FIG. 5. (a) Relative energy of E_{4f} with respect to the corresponding E_{4g} in $(\text{Ce}_{0.75}X_{0.25})_2\text{Fe}_{14}\text{B}$ ($X = \text{Sn}, \text{Sb}, \text{Pb}, \text{Bi}, \text{Ca}, \text{Sr}, \text{La}$, or Zr). (b) Calculated MAE in $\text{Ce}_2\text{Fe}_{14}\text{B}$, $(\text{Ce}_{0.75}X_{0.25})_2\text{Fe}_{14}\text{B}$ ($X = \text{Sn}, \text{Sb}, \text{Pb}, \text{Bi}, \text{La}$, and Zr), and $(\text{Ce}_{0.5}\text{Bi}_{0.5})_2\text{Fe}_{14}\text{B}$. Introduced Sn, Sb, Pb, Bi, and Zr atoms in (b) occupy the $4f$ site, and the La atoms in (b) are located at the $4g$ site.

slightly improved in the Sn-, Sb-, Pb-, and Zr-substituted cases, with percentages of less than 7%. The magnetic anisotropy in $\text{Ce}_2\text{Fe}_{14}\text{B}$ with La substitution is even smaller than that of pristine $\text{Ce}_2\text{Fe}_{14}\text{B}$, which should be related to the $4g$ -site occupation of La. However, the MAE of $(\text{Ce}_{0.75}\text{Bi}_{0.25})_2\text{Fe}_{14}\text{B}$ reaches 2.48 MJ/m^3 , which is 70% larger than the MAE in pristine $\text{Ce}_2\text{Fe}_{14}\text{B}$. Given that Bi substitution is effective at improving magnetic anisotropy, we further increase the Bi content to $(\text{Ce}_{0.5}\text{Bi}_{0.5})_2\text{Fe}_{14}\text{B}$, where all of the Bi atoms occupy the $4f$ site. It turns out that the MAE in $(\text{Ce}_{0.5}\text{Bi}_{0.5})_2\text{Fe}_{14}\text{B}$ can be up to 4.24 MJ/m^3 , which is almost 3 times the magnetic anisotropy in pristine $\text{Ce}_2\text{Fe}_{14}\text{B}$. We further calculate the atom-projected MAE for $(\text{Ce}_{0.5}\text{Bi}_{0.5})_2\text{Fe}_{14}\text{B}$, where the Bi-, Ce-, and Fe-projected MAEs are $3.40, 0.63$, and 0.50 MJ/m^3 , respectively. The large MAE contribution of Bi atoms should be associated with their strong SOC, which is scaled approximately by Z^4 ($Z = \text{atomic number}$) [43,44]. Moreover, in the order of listed systems in Fig. 5(b), the magnetizations of $(\text{Ce}_{0.75}X_{0.25})_2\text{Fe}_{14}\text{B}$ ($X = \text{Sn}, \text{Sb}$, and Bi) and $(\text{Ce}_{0.5}\text{Bi}_{0.5})_2\text{Fe}_{14}\text{B}$ are $1.56, 1.58, 1.58$, and 1.64 T , respectively, which are very close to the value of 1.53 T in $\text{Ce}_2\text{Fe}_{14}\text{B}$. Moreover, on the basis of $4.24 \text{ MJ/m}^3 K_1$ and 1.64 T magnetization in $(\text{Ce}_{0.5}\text{Bi}_{0.5})_2\text{Fe}_{14}\text{B}$, one can get the magnetic hardness parameter, κ , of 1.41 , which is greater than unity and the κ of 0.88 in $\text{Ce}_2\text{Fe}_{14}\text{B}$. These magnetic properties remind us that $(\text{Ce}_{0.5}\text{Bi}_{0.5})_2\text{Fe}_{14}\text{B}$ is promising as an inexpensive permanent magnet.

It should be noted that atom substitution in the rare-earth $4f$ site does not decrease the magnetization in $\text{Ce}_2\text{Fe}_{14}\text{B}$. On the contrary, the introduced Bi atoms slightly increase the magnetization of Fe atoms. We list the atomic spin and orbital moments of $(\text{Ce}_{0.5}\text{Bi}_{0.5})_2\text{Fe}_{14}\text{B}$ and $\text{Ce}_2\text{Fe}_{14}\text{B}$ in Table I. The moment differences of the

atomic spin (orbital) moment in $(\text{Ce}_{0.5}\text{Bi}_{0.5})_2\text{Fe}_{14}\text{B}$ and $\text{Ce}_2\text{Fe}_{14}\text{B}$ are defined as $\Delta\mu_S$ and $\Delta\mu_L$, as displayed in Fig. 6(a). All the spin and orbital moments of Fe atoms in $(\text{Ce}_{0.5}\text{Bi}_{0.5})_2\text{Fe}_{14}\text{B}$ are larger than that in $\text{Ce}_2\text{Fe}_{14}\text{B}$, Fe $4e$ shows the maximum $\Delta\mu_S$, and Fe $4c$ shows the maximum $\Delta\mu_L$. The increased magnetization in $(\text{Ce}_{0.5}\text{Bi}_{0.5})_2\text{Fe}_{14}\text{B}$ should be related to the d - p hybridization between Bi and Fe. Here, we analyze the partial DOS of $(\text{Ce}_{0.5}\text{Bi}_{0.5})_2\text{Fe}_{14}\text{B}$ and show the case of Fe $4c$ here as an example. As shown in the gray region of Fig. 6(b), the p -projected DOS in the Bi atom shows a similar contour to the d -orbital DOS of the Fe- $4c$ atom, underlining the d - p hybridization. Moreover, in the energy interval of [E_F – 4.8 eV , E_F – 3.8 eV], the p -projected DOS peak of Bi comes mainly from the p_x state (according to the inset of Fig. 6). Such a feature matches with the structural characteristic that Bi $4f$ and Fe $4c$ are located in the same x - y plane in the 2:14:1 structure.

TABLE I. Calculated spin (μ_S) and orbital (μ_L) magnetic moments on Ce, Bi, Fe, and B atoms in $\text{Ce}_2\text{Fe}_{14}\text{B}$ and $(\text{Ce}_{0.5}\text{Bi}_{0.5})_2\text{Fe}_{14}\text{B}$.

Atom	$\text{Ce}_2\text{Fe}_{14}\text{B}$		$(\text{Ce}_{0.5}\text{Bi}_{0.5})_2\text{Fe}_{14}\text{B}$	
	$\mu_S (\mu_B)$	$\mu_L (\mu_B)$	$\mu_S (\mu_B)$	$\mu_L (\mu_B)$
Ce $4f$ or Bi $4f$	-0.76	0.25	0.00	-0.02
Ce $4g$	-0.85	0.36	-0.78	0.39
Fe $4c$	2.45	0.04	2.50	0.07
Fe $4e$	1.99	0.04	2.18	0.05
Fe $8j1$	2.30	0.03	2.30	0.04
Fe $8j2$	2.73	0.04	2.80	0.04
Fe $16k1$	2.25	0.04	2.34	0.05
Fe $16k2$	2.35	0.04	2.41	0.05
B $4g$	-0.14	0.00	-0.16	0.00

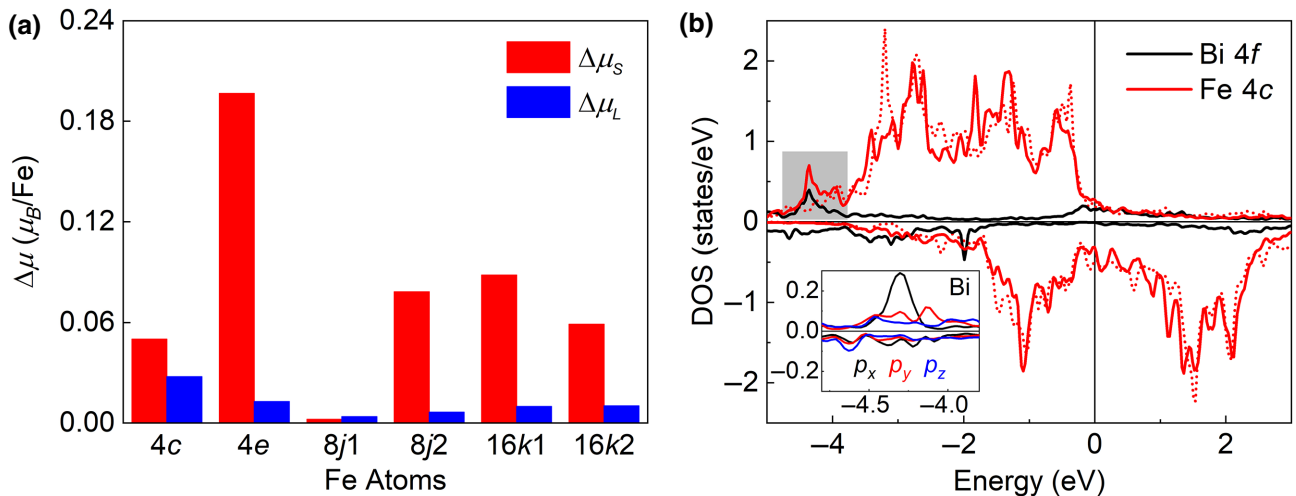


FIG. 6. (a) Spin (orbital) moment difference, $\Delta\mu$ (μ_B/Fe), of Fe atoms in $(\text{Ce}_{0.5}\text{Bi}_{0.5})_2\text{Fe}_{14}\text{B}$ and $\text{Ce}_2\text{Fe}_{14}\text{B}$. Positive value of the moment difference means a larger moment in $(\text{Ce}_{0.5}\text{Bi}_{0.5})_2\text{Fe}_{14}\text{B}$, as compared with $\text{Ce}_2\text{Fe}_{14}\text{B}$. (b) Spin-polarized DOS projected on p states in Bi-4f atom and d states of Fe-4c atom in $(\text{Ce}_{0.5}\text{Bi}_{0.5})_2\text{Fe}_{14}\text{B}$. Red dashed lines correspond to d -projected DOS of Fe-4c atom in $\text{Ce}_2\text{Fe}_{14}\text{B}$. Inset denotes the p -projected DOS of Bi-4f atom in $(\text{Ce}_{0.5}\text{Bi}_{0.5})_2\text{Fe}_{14}\text{B}$, in the energy interval of [$E_F-4.8$ eV, $E_F-3.8$ eV] as marked by the gray region. Fermi level is 0 eV.

Given the promising magnetic properties in $(\text{Ce}_{1-x}\text{Bi}_x)_2\text{Fe}_{14}\text{B}$, we try to fabricate Bi-substituted compounds. Unfortunately, we fail to synthesize Bi-doped $\text{Ce}_2\text{Fe}_{12.7}\text{Co}_{1.3}\text{B}$ via a conventional arc melting and postannealing process due to phase separation. We will try more methods later. Here, we estimate the thermodynamic stability of $(\text{Ce}_{0.5}\text{Bi}_{0.5})_2\text{Fe}_{14}\text{B}$ by the enthalpies of formation, ΔH_f , and potential decomposition enthalpies, ΔH_d , by the grand canonical linear programming method [45,46]. ΔH_f , on a per-atom basis, is calculated based on the elementary substances as follows:

$$\Delta H_f = [H((\text{Ce}_{0.5}\text{Bi}_{0.5})_2\text{Fe}_{14}\text{B}) - H(\text{Ce}) - H(\text{Bi}) - 14H(\text{Fe}) - H(\text{B})]/17, \quad (1)$$

where the applied enthalpy denotes the total enthalpy of related materials. The enthalpies of Ce, Bi, Fe, and B are calculated in their stable phases in the Materials Project database [47–49]. As listed in Table II, the calculated ΔH_f of 0.028 eV/atom in $(\text{Ce}_{0.5}\text{Bi}_{0.5})_2\text{Fe}_{14}\text{B}$ is higher than that in $\text{Ce}_2\text{Fe}_{14}\text{B}$. Given that the system with a lower formation enthalpy will be more stable at high temperatures, $(\text{Ce}_{0.5}\text{Bi}_{0.5})_2\text{Fe}_{14}\text{B}$ seems to be unstable with respect to the formation of $\text{Ce}_2\text{Fe}_{14}\text{B}$. However, the $R_2\text{Fe}_{14}\text{B}$ structure could be formed with $R = \text{Y}, \text{Th}$, and all the lanthanide elements except Eu and Pm. The formation enthalpies of these $R_2\text{Fe}_{14}\text{B}$ materials range from -0.125 eV/atom (in $\text{Lu}_2\text{Fe}_{14}\text{B}$) to 0.727 eV/atom (in $\text{Gd}_2\text{Fe}_{14}\text{B}$). Parts of $R_2\text{Fe}_{14}\text{B}$ are listed in Table II. So, it is entirely possible that $(\text{Ce}_{0.5}\text{Bi}_{0.5})_2\text{Fe}_{14}\text{B}$, with ΔH_f of 0.028 eV/atom, may form under appropriate synthesis conditions.

We now assess the potential decomposition of $(\text{Ce}_{0.5}\text{Bi}_{0.5})_2\text{Fe}_{14}\text{B}$, with ternary and binary compounds with Bi, Ce, Fe, or B atoms, as summarized in the Materials Project database. According to the database, there are no Bi-Fe-B, Bi-Ce-Fe, or Bi-Ce-B ternary compounds. So, we further check the Bi-based binary compounds with Ce, Fe, or B. It turns out that the Bi-Fe compound does not exist, and none of the listed Bi-B compounds are stable. Finally, the Bi-Ce binary compounds are used to assess decomposition. All the stable Bi-Ce compounds are listed in Table II, where CeBi holds the lowest formation enthalpy. So, we employ CeBi as the secondary phases and assess the decomposition as follows:

$$\Delta H_d = [H((\text{Ce}_{0.5}\text{Bi}_{0.5})_2\text{Fe}_{14}\text{B}) - H(\text{CeBi}) - H(\text{FeB}) - 13H(\text{Fe})]/17, \quad (2)$$

$$\Delta H_d = [H((\text{Ce}_{0.5}\text{Bi}_{0.5})_2\text{Fe}_{14}\text{B}) - H(\text{CeBi}) - 14H(\text{Fe}) - H(\text{B})]/17. \quad (3)$$

The calculated decomposition enthalpy, ΔH_d , of $(\text{Ce}_{0.5}\text{Bi}_{0.5})_2\text{Fe}_{14}\text{B}$ is 0.165 eV/atom from Eq. (2) and 0.121 eV/atom from Eq. (3), which is larger than the ΔH_d of $\text{Ce}_2\text{Fe}_{14}\text{B}$ but smaller than those of $\text{Pr}_2\text{Fe}_{14}\text{B}$ and $\text{Nd}_2\text{Fe}_{14}\text{B}$. So, $(\text{Ce}_{0.5}\text{Bi}_{0.5})_2\text{Fe}_{14}\text{B}$ is still possible to prepare in experiments.

Moreover, in analogy to $(\text{Ce}_{0.5}\text{Bi}_{0.5})_2\text{Fe}_{14}\text{B}$, we also calculate ΔH_f and ΔH_d for $(\text{Ce}_{0.75}\text{Bi}_{0.25})_2\text{Fe}_{14}\text{B}$, as described by

$$\Delta H_f = [H((\text{Ce}_{0.75}\text{Bi}_{0.25})_2\text{Fe}_{14}\text{B}) - 1.5H(\text{Ce}) - 0.5H(\text{Bi}) - 14H(\text{Fe}) - H(\text{B})]/17, \quad (4)$$

TABLE II. Enthalpies of formation (ΔH_f), decompositions, and related decomposition enthalpies (ΔH_d) of $(\text{Ce}_{0.5}\text{Bi}_{0.5})_2\text{Fe}_{14}\text{B}$, $R_2\text{Fe}_{14}\text{B}$ ($R = \text{Ce}, \text{Pr}, \text{Nd}, \text{Sm}, \text{or Gd}$) and stable binary compounds with Ce, Bi, Fe, or B atoms in Materials Project database. $\text{Ce}(\text{FeB})_4$ is also listed, as one of the decomposition materials of $\text{Ce}_2\text{Fe}_{14}\text{B}$.

Compound	ΔH_f (eV/atom)	Decompose to	ΔH_d (eV/atom)
$(\text{Ce}_{0.5}\text{Bi}_{0.5})_2\text{Fe}_{14}\text{B}$	0.028	Discussed	Discussed
$\text{Ce}_2\text{Fe}_{14}\text{B}$	-0.071	$\text{Ce}(\text{FeB})_4 + \text{CeFe}_2 + \text{Fe}$	0.019
$\text{Pr}_2\text{Fe}_{14}\text{B}$	0.218	$\text{Pr}(\text{FeB})_4 + \text{Pr} + \text{Fe}$	0.273
$\text{Nd}_2\text{Fe}_{14}\text{B}$	0.190	$\text{Nd}(\text{FeB})_4 + \text{Nd} + \text{Fe}$	0.247
$\text{Sm}_2\text{Fe}_{14}\text{B}$	-0.078	Stable	...
$\text{Gd}_2\text{Fe}_{14}\text{B}$	0.727	$\text{Gd}_2\text{Fe}_{17} + \text{GdFe}_4\text{B} + \text{Fe}$	0.800
CeBi	-0.813	Stable	...
CeBi_3	-0.439	Stable	...
Ce_2Bi	-0.547	Stable	...
Ce_4Bi_3	-0.702	Stable	...

$$\Delta H_d = [H((\text{Ce}_{0.75}\text{Bi}_{0.25})_2\text{Fe}_{14}\text{B}) - 0.5H(\text{CeBi}) - H(\text{Ce}) - H(\text{FeB}) - 13H(\text{Fe})]/17, \quad (5)$$

$$\Delta H_d = [H((\text{Ce}_{0.75}\text{Bi}_{0.25})_2\text{Fe}_{14}\text{B}) - 0.5H(\text{CeBi}) - H(\text{Ce}) - 14H(\text{Fe}) - H(\text{B})]/17. \quad (6)$$

According to Eq. (4), the calculated ΔH_f is negative, with a value of -0.027 eV/atom. The ΔH_d of $(\text{Ce}_{0.75}\text{Bi}_{0.25})_2\text{Fe}_{14}\text{B}$ is calculated to be 0.065 eV/atom from Eq. (5) and 0.020 eV/atom from Eq. (6); these values are lower than those of 0.165 and 0.121 eV/atom in $(\text{Ce}_{0.5}\text{Bi}_{0.5})_2\text{Fe}_{14}\text{B}$. These results underline that $(\text{Ce}_{0.75}\text{Bi}_{0.25})_2\text{Fe}_{14}\text{B}$ should be more stable than $(\text{Ce}_{0.5}\text{Bi}_{0.5})_2\text{Fe}_{14}\text{B}$. Hence, we suggest that a low content of Bi is a good starting choice for fabricating Bi-substituted $\text{Ce}_2\text{Fe}_{14}\text{B}$ in later experiments.

Moreover, in addition to magnetic anisotropy and saturation magnetization, the Curie point is an indispensable property for permanent-magnet applications. As reported previously, in $\text{Ce}_2\text{Fe}_{14}\text{B}$, the Curie temperature increases with the Co content, up to a maximum of 586 K at a Co content of about 15% [37]. On that basis, Co substitution may be employed in $(\text{Ce}_{0.75}\text{Bi}_{0.25})_2\text{Fe}_{14}\text{B}$ and $(\text{Ce}_{0.5}\text{Bi}_{0.5})_2\text{Fe}_{14}\text{B}$ for a higher Curie point. So, we calculate magnetization and anisotropy for the two Bi cases with Co contents of 10% and 15% by employing the virtual-crystal approximation to treat the $\text{Fe}(\text{Co})$ disorder. We find that the magnetizations of the two Bi cases are almost unaffected by the introduced Co. The magnetic anisotropy of 2.48 MJ/m^3 in $(\text{Ce}_{0.75}\text{Bi}_{0.25})_2\text{Fe}_{14}\text{B}$ decreases to 1.80 MJ/m^3 with 10% Co and 2.18 MJ/m^3 with 15% Co. While, for $(\text{Ce}_{0.5}\text{Bi}_{0.5})_2\text{Fe}_{14}\text{B}$, the magnetic anisotropy of 4.24 MJ/m^3 becomes 3.77 MJ/m^3 with 10% Co and 3.82 MJ/m^3 with 15% Co. It can be roughly assessed that the magnetic anisotropies of the two Bi cases decrease by 10–12% upon proper Co substitution. So, although Co substitution decreases the magnetic anisotropy in the two Bi cases, it is still possible to control the magnetic anisotropy by optimizing the content of Co.

These results lay the foundation for low-cost $\text{Ce}_2\text{Fe}_{14}\text{B}$ -based permanent-magnet applications.

We also wish to note that, even for magnetic anisotropy fields at about 3-tesla room-temperature values we find experimentally, it should still be feasible to make rather high-performance magnets in this class. Relying on the time-tested Brown paradox [2], in which experimentally realizable coercivities can be as high as 30% of the anisotropy field, results in estimated coercivities as high as 0.9 T, which exceeds half the approximate 1.4-T room-temperature magnetization of these alloys. This would thus allow these magnets to be made in any shape free of demagnetization effects and obtain a full-energy product as high as 38 MG Oe. Although not studied here, previous work [3] has also found that, in $\text{Ce}_2\text{Fe}_{14}\text{B}$ and $\text{La}_2\text{Fe}_{14}\text{B}$, anisotropy fields are nearly constant in the technologically important range just above room temperature, rather than falling off quickly with temperature, as in $\text{Nd}_2\text{Fe}_{14}\text{B}$. It is this latter property that largely necessitates the unfavorable usage of extremely critical and expensive Dy to fix anisotropy deterioration at high temperatures in these latter magnets. Ce-substituted $\text{Nd}_2\text{Fe}_{14}\text{B}$ is also demonstrated as an alternative to expensive Dy-containing high-performance $\text{Nd}_2\text{Fe}_{14}\text{B}$ -based magnets [50]. The suggestion is therefore that, when it becomes possible to fabricate $\text{Ce}_2\text{Fe}_{14}\text{B}$ -based magnets, as considered here, it is likely that such magnets will not require the rather inelegant and expensive Dy-based “fix” that Nd-based magnets presently require, which substantially reduces room-temperature energy products.

We do not claim here that $\text{Ce}_2\text{Fe}_{14}\text{B}$ -based magnets are likely to become fully competitive with $\text{Nd}_2\text{Fe}_{14}\text{B}$ (the magnetic anisotropy, for one, is smaller than optimal for this purpose), but rather to point out that it should be possible to make highly useful permanent magnets in this family at greatly reduced cost and criticality relative to $\text{Nd}_2\text{Fe}_{14}\text{B}$. For comparison, the present price of neodymium oxide is approximately \$150/kilo (see relevant information at Ref. [52]), while that of cerium and lanthanum is

approximately \$2/kilo. With regards to the cost of cobalt, the use of just 7 wt% cobalt (as in our proposed LaCeFe_{12.7}Co_{1.3}B alloy), even at present historic cobalt prices of \$80/kilo, adds only about \$5/kilo to the material's cost. Much the same logic is employed for (Fe_{1-x}Co_x)₂B alloys [51]. Due to significant, though clearly not competitive with Nd₂Fe₁₄B, magnetic anisotropy, we find that energy products as high as 38 MG Oe are plausible in these alloys at minimal material costs.

IV. CONCLUSION

We experimentally study the magnetic properties of Ce₂Fe₁₄B with Co, La, and Zr substitutions. Together with Co substitutions of Fe, partial Zr substitution increases the impurity phase and has little effect on the Curie point and M_s . While, without loss of the anisotropy field, substitution of La improves the Curie temperature and M_s , which may produce an estimated energy product as high as 38 MG Oe. These properties enable LaCeFe_{12.7}Co_{1.3}B as a potential critical-element-free high-performance permanent magnet. We further study the origin of magnetic anisotropy in Ce₂Fe₁₄B from first principles. It turns out that the magnetic anisotropy of Ce₂Fe₁₄B is comparably contributed to by the Ce and Fe atoms. Then the Ce-projected magnetic anisotropy is predominately provided by the Ce atoms at the 4g site. Particularly, employing the Bi substitution of Ce atoms at the 4f site can increase the magnetic anisotropy energy to 4.24 MJ/m³ in (Ce_{0.5}Bi_{0.5})₂Fe₁₄B, which is almost 3 times that in Ce₂Fe₁₄B. Meanwhile, (Ce_{0.5}Bi_{0.5})₂Fe₁₄B has a strong magnetization of 1.64 T and a magnetic hardness parameter of 1.41. These magnetic criteria also imply the potential of Bi substitution for making Ce₂Fe₁₄B a low-cost high-performance permanent magnet. Our experimental and theoretical results provide a foundation for developing Ce₂Fe₁₄B-based critical-element-free high-performance low-cost permanent magnets.

ACKNOWLEDGEMENTS

This research is supported by the Critical Materials Institute, an Energy Innovation Hub funded by the U.S. Department of Energy (DOE), Office of Energy Efficiency and Renewable Energy, Advanced Manufacturing Office. This research uses resources of the Compute and Data Environment for Science (CADES) at the Oak Ridge National Laboratory (ORNL), which is supported by the Office of Science of the U.S. Department of Energy under contract No. DE-AC05-00OR22725. The U.S. Government retains, and the publisher, by accepting the article for publication, acknowledges that the U.S. Government retains a nonexclusive, paid-up, irrevocable, worldwide license to publish or reproduce the published form of this manuscript, or allow others to do so for U.S. Government purposes. The Department of Energy will provide public

access to these results of federally sponsored research in accordance with the DOE Public Access Plan [53].

- [1] J. M. D. Coey, Hard magnetic materials: A perspective, *IEEE Trans. Magn.* **47**, 4671 (2011).
- [2] D. Goll and H. Kronmüller, High-performance permanent magnets, *Naturwissenschaften* **87**, 423 (2000).
- [3] J. F. Herbst, R₂Fe₁₄B materials: Intrinsic properties and technological aspects, *Rev. Mod. Phys.* **63**, 819 (1991).
- [4] J. M. D. Coey, Permanent magnets: Plugging the gap, *Scr. Mater.* **67**, 524 (2012).
- [5] L. Yin, R. Juneja, L. Lindsay, T. Pandey, and D. S. Parker, Semihard Iron-Based Permanent-Magnet Materials, *Phys. Rev. Appl.* **15**, 024012 (2021).
- [6] T. N. Lamichhane, M. T. Onysczak, O. Palasyuk, S. Sharikadze, T. Kim, Q. Lin, M. J. Kramer, R. W. McCallum, A. L. Wysocki, M. C. Nguyen, *et al.*, Single-Crystal Permanent Magnets: Extraordinary Magnetic Behavior in the Ta-, Cu-, and Fe-Substituted CeCo₅ Systems, *Phys. Rev. Appl.* **11**, 014052 (2019).
- [7] T. N. Lamichhane, V. Taufour, A. Palasyuk, Q. Lin, S. L. Bud'ko, and P. C. Canfield, Ce_{3-x}Mg_xCo₉: Transformation of a Pauli Paramagnet into a Strong Permanent Magnet, *Phys. Rev. Appl.* **9**, 024023 (2018).
- [8] T. Pandey and D. S. Parker, Borderline Magnetism: How Adding Mg to Paramagnetic CeCo₃ Makes a 450-K Ferromagnet with Large Magnetic Anisotropy, *Phys. Rev. Appl.* **10**, 034038 (2018).
- [9] T. Pandey and D. S. Parker, Potential High-Performance Magnet: Fe- and Zr-Alloyed Ce₂Co₁₇, *Phys. Rev. Appl.* **13**, 034039 (2020).
- [10] Hİ Sözen, S. Ener, F. Maccari, K. P. Skokov, O. Gutfleisch, F. Körmann, J. Neugebauer, and T. Hickel, Ab initio phase stabilities of Ce-based hard magnetic materials and comparison with experimental phase diagrams, *Phys. Rev. Mater.* **3**, 084407 (2019).
- [11] L. Yin and D. S. Parker, Effect of atom substitutions on the magnetic properties in Ce₂Fe₁₇: Toward permanent magnet applications, *J. Appl. Phys.* **129**, 103902 (2021).
- [12] A. V. Andreev, D. Rafaja, J. Kamarad, Z. Arnold, Y. Homma, and Y. Shiokawa, Magnetic properties of Lu₂Fe₁₇ crystals, *J. Alloys Compd.* **361**, 48 (2003).
- [13] S. A. Nikitin, I. S. Tereshina, N. Y. Pankratov, E. A. Tereshina, Y. V. Skourski, K. P. Skokov, and Y. G. Pastushenkov, Magnetic anisotropy and magnetostriction in a Lu₂Fe₁₇ intermetallic single crystal, *Phys. Solid State* **43**, 1720 (2001).
- [14] Y. Makihara, Y. Uwatoko, H. Matsuoka, M. Kosaka, H. Fukuda, and H. Fujii, Magnetism in single crystal Ce₂Fe₁₇ with two types of magnetic ground states, *J. Magn. Magn. Mater.* **272-276**, 551 (2004).
- [15] Z. Li, M. Yue, X. Liu, H. Zhang, W. Liu, Y. Li, and Z. Zhang, Tuning the structure and intrinsic magnetic properties of Ce₂Fe₁₄B alloys by elimination of CeFe₂ with La substitution, *J. Magn. Magn. Mater.* **505**, 166747 (2020).
- [16] K. Orimoloye, D. H. Ryan, F. E. Pinkerton, and M. Medraj, Intrinsic magnetic properties of Ce₂Fe₁₄B modified by Al, Ni, or Si, *Appl. Sci.* **8**, 205 (2018).

- [17] J. Zhang, L. Zhao, X. Liao, H. Zeng, and Z. Liu, in *2018 IEEE International Magnetics Conference (INTERMAG)* (2018), p. 1.
- [18] T. W. Capehart, R. K. Mishra, and F. E. Pinkerton, Determination of the zirconium site in zirconium-substituted $\text{Nd}_2\text{Fe}_{14}\text{B}$, *J. Appl. Phys.* **73**, 6476 (1993).
- [19] M. Jurczyk and W. E. Wallace, Magnetic behavior of $\text{R}1.9\text{Zr}0.1\text{Fe}14\text{B}$ and $\text{R}1.9\text{Zr}0.1\text{Fe}12\text{Co}2\text{B}$ compounds, *J. Magn. Magn. Mater.* **59**, L182 (1986).
- [20] D. Haskel, J. C. Lang, Z. Islam, A. Cady, G. Srajer, M. van Veenendaal, and P. C. Canfield, Atomic Origin of Magnetocrystalline Anisotropy in $\text{Nd}_2\text{Fe}_{14}\text{B}$, *Phys. Rev. Lett.* **95**, 217207 (2005).
- [21] B. C. Sales, B. Saparov, M. A. McGuire, D. J. Singh, and D. S. Parker, Ferromagnetism of Fe_3Sn and alloys, *Sci. Rep.* **4**, 7024 (2014).
- [22] E. Sjöstedt, L. Nordström, and D. J. Singh, An alternative way of linearizing the augmented plane-wave method, *Solid State Commun.* **114**, 15 (2000).
- [23] P. Blaha, K. Schwarz, G. K. H. Madsen, D. Kvasnicka, and J. Luitz, *WIEN2K, an augmented plane wave + local orbitals program for calculating crystal properties* (Technische Universität Wien, Vienna, 2001).
- [24] J. P. Perdew, K. Burke, and M. Ernzerhof, Generalized Gradient Approximation Made Simple, *Phys. Rev. Lett.* **77**, 3865 (1996).
- [25] D. J. Singh and L. Nordstrom, *Planewaves pseudopotentials and the LAPW method*, 2nd ed. (Springer, Berlin, 2006).
- [26] S. Hirosawa, Y. Matsuura, H. Yamamoto, S. Fujimura, M. Sagawa, and H. Yamauchi, Magnetization and magnetic anisotropy of $\text{R}_2\text{Fe}_{14}\text{B}$ measured on single crystals, *J. Appl. Phys.* **59**, 873 (1986).
- [27] J. F. Herbst and W. B. Yelon, Crystal and magnetic structure of $\text{Ce}_2\text{Fe}_{14}\text{B}$ and $\text{Lu}_2\text{Fe}_{14}\text{B}$, *J. Magn. Magn. Mater.* **54–57**, 570 (1986).
- [28] R. Skomski and J. M. D. Coey, Magnetic anisotropy—how much is enough for a permanent magnet?, *Scr. Mater.* **112**, 3 (2016).
- [29] A. Vishina, O. Y. Vekilova, T. Björkman, A. Bergman, H. C. Herper, and O. Eriksson, High-throughput and data-mining approach to predict new rare-earth free permanent magnets, *Phys. Rev. B* **101**, 094407 (2020).
- [30] K. Momma and F. Izumi, VESTA 3 for three-dimensional visualization of crystal, volumetric and morphology data, *J. Appl. Crystallogr.* **44**, 1272 (2011).
- [31] G. Kresse and J. Furthmüller, Efficiency of ab-initio total energy calculations for metals and semiconductors using a plane-wave basis set, *Comput. Mater. Sci.* **6**, 15 (1996).
- [32] G. Kresse and J. Furthmüller, Efficient iterative schemes for ab initio total-energy calculations using a plane-wave basis set, *Phys. Rev. B* **54**, 11169 (1996).
- [33] P. E. Blöchl, Projector augmented-wave method, *Phys. Rev. B* **50**, 17953 (1994).
- [34] G. Kresse and D. Joubert, From ultrasoft pseudopotentials to the projector augmented-wave method, *Phys. Rev. B* **59**, 1758 (1999).
- [35] C. Abache and H. Oesterreicher, Structural and magnetic properties of $\text{R}_2\text{Fe}_{14-x}\text{T}_x\text{B}$ ($\text{R} = \text{Nd}, \text{Y}$; $\text{T} = \text{Cr}, \text{Mn}, \text{Co}, \text{Ni}, \text{Al}$), *J. Appl. Phys.* **60**, 1114 (1986).
- [36] M. Jurczyk, Magnetic and crystallographic properties of substituted didymium $_{2-x}\text{Fe}_{12-x}\text{T}_x\text{Co}_2\text{B}$ compounds ($\text{T} = \text{Si}, \text{V}, \text{Cr}, \text{Ta}$ and W), *J. Magn. Magn. Mater.* **73**, 367 (1988).
- [37] T. Wang and M. Medraj, Intrinsic magnetic properties of $\text{Ce}_2(\text{Fe}, \text{Co})_{14}\text{B}$ and its modifications by Ni and Cu, *J. Alloys Compd.* **763**, 916 (2018).
- [38] T. Wang and M. Medraj, Magnetic force microscopic study of $\text{Ce}_2(\text{Fe}, \text{Co})_{14}\text{B}$, and its modifications by Ni and Cu, *J. Magn. Magn. Mater.* **460**, 95 (2018).
- [39] T. W. Capehart, R. K. Mishra, G. P. Meissner, C. D. Fuerst, and J. F. Herbst, Steric variation of the cerium valence in $\text{Ce}_2\text{Fe}_{14}\text{B}$ and related compounds, *Appl. Phys. Lett.* **63**, 3642 (1993).
- [40] J. Wang, L. Liang, L. T. Zhang, M. Yano, K. Terashima, H. Kada, S. Kato, T. Kadono, S. Imada, T. Nakamura, *et al.*, Mixed-valence state of Ce and its individual atomic moments in $\text{Ce}_2\text{Fe}_{14}\text{B}$ studied by soft x-ray magnetic circular dichroism, *Intermetallics* **69**, 42 (2016).
- [41] J. Jin, Y. Zhang, G. Bai, Z. Qian, C. Wu, T. Ma, B. Shen, and M. Yan, Manipulating Ce valence in $\text{RE}_2\text{Fe}_{14}\text{B}$ tetragonal compounds by La-Ce Co-doping: Resultant crystallographic and magnetic anomaly, *Sci. Rep.* **6**, 30194 (2016).
- [42] C. N. Singman, Atomic volume and allotropy of the elements, *J. Chem. Educ.* **61**, 137 (1984).
- [43] C. Du, H. Wang, F. Yang, and P. C. Hammel, Systematic variation of spin-orbit coupling with *d*-orbital filling: Large inverse spin Hall effect in 3*d* transition metals, *Phys. Rev. B* **90**, 140407 (2014).
- [44] D. D. Sarma, Nature of dependence of spin-orbit splittings on atomic number, *Proc. Indian Acad. Sci.* **90**, 19 (1981).
- [45] A. R. Akbarzadeh, V. Ozoliņš, and C. Wolverton, First-principles determination of multicomponent hydride phase diagrams: Application to the Li-Mg-N-H system, *Adv. Mater.* **19**, 3233 (2007).
- [46] Y. Wang, Y. Zhang, and C. Wolverton, First-principles studies of phase stability and crystal structures in Li-Zn mixed-metal borohydrides, *Phys. Rev. B* **88**, 024119 (2013).
- [47] A. Jain, S. P. Ong, G. Hautier, W. Chen, W. D. Richards, S. Dacek, S. Cholia, D. Gunter, D. Skinner, G. Ceder, *et al.*, Commentary: The Materials Project: A materials genome approach to accelerating materials innovation, *APL Mater.* **1**, 011002 (2013).
- [48] A. Jain, G. Hautier, S. P. Ong, C. J. Moore, C. C. Fischer, K. A. Persson, and G. Ceder, Formation enthalpies by mixing GGA and GGA + *U* calculations, *Phys. Rev. B* **84**, 045115 (2011).
- [49] S. P. Ong, L. Wang, B. Kang, and G. Ceder, Li–Fe–P–O₂ phase diagram from first principles calculations, *Chem. Mater.* **20**, 1798 (2008).
- [50] A. K. Pathak, K. A. Gschneidner, M. Khan, R. W. McCallum, and V. K. Pecharsky, High performance Nd-Fe-B permanent magnets without critical elements, *J. Alloys Compd.* **668**, 80 (2016).
- [51] M. D. Kuz'min, K. P. Skokov, H. Jian, I. Radulov, and O. Gutfleisch, Towards high-performance permanent magnets without rare earths, *J. Phys. Condens. Matter* **26**, 064205 (2014).
- [52] <https://www.metal.com/Rare-Earth-Oxides>
- [53] <http://energy.gov/downloads/doe-public-access-plan>